# Continuous Monitoring of Crop Reflectance, Vegetation Fraction, and Identification of Developmental Stages Using a Four Band Radiometer

Anthony Nguy-Robertson, Anatoly Gitelson,* Yi Peng, Elizabeth Walter-Shea, Bryan Leavitt, and Timothy Arkebauer

## ABSTRACT

**Real-time monitoring of crop vegetation fraction and identification of development stages provides useful information for crop management. Using sensors at close range makes it possible to collect data with very high temporal resolution. This study used four-band radiometers with green, red, red edge, and near infrared spectral bands for daily monitoring of maize (*Zea mays* L.) and soybean [*Glycine max* (L.) Merr.] reflectance during the growing season in three fields over 3 yr. Two fields were continuous irrigated maize and the third was managed under a maize/soybean rotation. The objectives were (i) determine diurnal and seasonal temporal behavior of reflectance in two contrasting crops, maize and soybean, (ii) remotely estimate the crop developmental stage using spectral spaces and vegetation indices, and (iii) estimate vegetation fraction using spectral spaces. Diurnal reflectance behavior indicated that the median reflectance measured within 2.5 h of solar noon was reliable for examining the daily behavior of reflectance and vegetation indices. Since the information content of reflectance in different spectral bands varies over the course of a season, spectral spaces (reflectance in one band vs. reflectance in another band) were constructed and shown to be a useful tool for identifying crop developmental stages. Five distinct stages of vegetation status (soil/residue, green-up, vegetative, senescence, and soil/stover/residue) were accurately identified using the red vs. green reflectance spectral space. Vegetation fraction was estimated using spectral spaces in maize with estimation error below 0.071 and in soybean below 0.064. Thus, high temporal resolution sensors can be a reliable tool for monitoring vegetation for a variety of applications.**

Given the current interest in quantifying impacts of climate change (Richardson et al., 2009; Hufkens et al., 2012), real-time monitoring of changes in the stage of plant development or "shifts in seasonal timing" as defined by the U.S. National Phenological Network (Betancourt et al., 2005) is of importance. These plant development stages represent broad phenological phases in contrast to the "physiological and morphological stage of plant development" as defined by Hanway (1963). Earlier studies have attempted to achieve near-continuous data sets for monitoring phenology and crop developmental stages by collecting data frequently (two to three times per week) using a close range spectroradiometer (Goodin and Henebry, 1997; Viña et al., 2004). However, even with these frequent measurements, critical features in phenology may be missed if the date of acquisition does not coincide with the feature of interest (Cleary and Waring, 1969; Ramsey, 1995). Therefore, instruments that are capable of collecting data continuously have been used recently for monitoring broad phenological changes and physiological status of vegetation. Instruments with appropriate infrastructure that can be setup to collect high temporal data include light emitting diodes, LEDs (Ryu et al., 2010), radiometers (Eklundh et al., 2011), and digital cameras (Sakamoto et al., 2012).

One of the advantages of using a high temporal resolution sensor is the ability to examine the diurnal behavior of reflectance in addition to the behavior of the daily reflectance throughout the growing season. Most studies report the typical behavior of reflectance (Idso and de Wit, 1970; Pinter, 1986) and of vegetation indices (VIs) (Zarco-Tejada, 2000); however, there are many factors that may impact reflectance and thus VIs, such as solar angles (Liang et al., 2003; de Souza et al., 2010), periods of stress (Gamon and Bond, 2013), etc. By having a high temporal sensor, these different factors can be examined. Most studies using daily measurements of reflectance have used different VIs, which are mathematical combinations of spectral bands, to track broad phenological and crop developmental stages (Soudani et al., 2012; Huete, 2012). However, when applied to data with lower temporal resolution, this approach has some limitations without knowledge of the context of the data set or the aid of ancillary data. For example, with the same crop greenness, the values of most typically used VIs (e.g., normalized difference vegetation index, NDVI)

A. Nguy-Robertson, A. Gitelson, Y. Peng, and B. Leavitt, Center for Advanced Land Management Information Technologies, School of Natural Resources, University of Nebraska-Lincoln, Lincoln, NE 688588-0973; A. Nguy-Robertson, A. Gitelson, Y. Peng, E. Walter-Shea, and B. Leavitt, School of Natural Resources, University of Nebraska-Lincoln, Lincoln, NE 688588-0973; and T. Arkebauer, Department of Agronomy and Horticulture, University of Nebraska-Lincoln, Lincoln, NE 68583-0817. Received 14 May 2013. *Corresponding author (agitelson2@unl.edu).

Published in Agron. J. 105:1769–1779 (2013)
doi:10.2134/agronj2013.0242


**Abbreviations:** %PARpotential, percentage of photosynthetically active radiation; 2-D, two-dimensional; DW, downwelling irradiance; DOY, day of year; EVI, enhanced vegetation index; GDD, growing degree day; LAI, green leaf area index; NDVI, normalized difference vegetation index; PARin, incoming photosynthetically active radiation; PARpotential, potential photosynthetically active radiation; UNL, University of Nebraska-Lincoln; UW, upwelling radiance; VARI, visible atmospherically resistant index; VI, vegetation index

do not distinguish between the green-up/leaf-on and senescence stages. The ability to distinguish between the green-up and senescence stages will be especially important for interpretation of satellite data over regions where multiple cropping is common.

Spectral spaces, that is, relationships between reflectances in different spectral bands, can provide additional information, from that gained from VIs, about the phenological and physiological status of vegetation. For example, the tasseled cap methodology uses various reflectance bands in a 3-dimensional (3-D) space for a variety of applications such as estimating phenology (Crist and Kauth, 1986), differentiating between sagebrush species (Sivanpillai and Ewers, 2013), and informing models for predicting wildlife corridors (Squires et al., 2013). Two-dimensional (2-D) spectral spaces have been used to provide information on the impact of background on the overall reflectance (Gobron et al., 1999; Broge and Leblanc, 2001), as well as estimates of land cover (Hansen et al., 1998) and vegetation fraction (Gitelson et al., 2002b). The 2-D spectral spaces have also been used to estimate phenology, primarily by using the near infrared (NIR) vs. red reflectance space (Ayyangar et al., 1980). Less attention has been paid to the use of 2-D spectral spaces with visible spectral bands where in addition to a soil line, a vegetation line was clearly defined (Gitelson et al., 2002b).

The overall goal of this study was to investigate the utility of daily remotely sensed reflectance for crop monitoring. Specific objectives were to (i) study the diurnal and seasonal temporal behavior of reflectance in two contrasting (leaf structure and canopy architecture) crops, maize and soybean, (ii) remotely identify the crop developmental stages of maize and soybean using spectral spaces and VIs, and (iii) estimate vegetation fraction in both crops using spectral spaces in visible range.

## MATERIALS AND METHODS

### General Characteristics of the Study Area

The study area included three approximately 65-ha fields involved in the Carbon Sequestration Program (Verma et al., 2005) located at the University of Nebraska-Lincoln (UNL) Agricultural Research and Development Center near Mead, NE, (41°10′46.8″N, 96°26′22.7″W, 361 m above mean sea level) under different management conditions. During the duration of this study, 2010 to 2012, two of the fields were irrigated maize and the third was a rainfed maize/soybean rotation. All fields were fertilized and treated with herbicide/pesticides following UNL's best management practices for eastern Nebraska. A summary of the hybrids, planting densities, and maximal green leaf area index (LAI) is in Table 1. The row spacing was 76 cm for all fields and the rows were planted in an east–west orientation. Additional details on the study sites can be found in Verma et al. (2005) and Suyker et al. (2005).

The LAI was calculated from the leaf area determined from plants harvested from a 1 m length of one or two rows (6±2 plants) from six small (20 by 20 m) plots established in each field. These plots represented all major soil types within the field. The plants were collected every 10 to 14 d from each field between emergence and crop maturity (with the exception of the 2010 season which ended after day of year [DOY] 255 due to loss of power to the instruments and heavy crop damage following a hail storm). The plants collected were transported on ice to the laboratory for visual separation into green and dead leaves. The leaf area of the green leaves per plant was measured using an area meter (LI-3100, Li-Cor, Lincoln, NE). The LAI was determined by multiplying the green leaf area per plant by the plant population (plants $m^{-2}$) within the sampling plot. The LAI values from all six plots were averaged to provide a field-level LAI. Crop phenological stage (Abendroth et al., 2011) was also recorded for each plot on each LAI sampling date.

**Table 1. Hybrid, planting density and maximum green leaf area index (LAI) at the three Mead, NE, study sites from 2010 to 2013.**

| Year | Site | Crop | Hybrid | Planting density | Maximum LAI |
|---|---|---|---|---|---|
| | | | | plants $ha^{-1}$ | $m^2$ $m^{-2}$ |
| 2010 | 1 | maize | DeKalb 65–63 VT3 | 81,675 | 5.67 |
| | 2 | maize | DeKalb 65–63 VT3 | 82,382 | 4.54 |
| | 3 | soybean | Pioneer 93M11 | 370,644 | 3.76 |
| 2011 | 1 | maize | Pioneer 32T88 | 80,153 | 5.75 |
| | 2 | maize | Pioneer 32T88 | 81,112 | 6.11 |
| | 3 | maize | DeKalb 61–69 VT3 | 56,834 | 3.49 |
| 2012 | 1 | maize | DeKalb 62–97 VT3 | 84,015 | 4.66 |
| | 2 | maize | DeKalb 62–97 VT3 | 84,015 | 4.96 |
| | 3 | soybean | Pioneer 93M43 | 370,644 | 3.31 |

### Radiometer Calibration Procedures

Seven SKYE radiometers (SKR 1850, SKYE Instruments Ltd, Llandrindod Wells, UK), with four spectral bands were employed: green (536.5–561.5 nm), red (664.5–675.5 nm), red edge (704.5–715.5 nm), and NIR (862–874 nm). SKYE radiometers can measure downwelling irradiance (DW) with the aid of a cosine corrector, which collects light in 180° hemisphere above the sensor, according to Lambert's cosine law, to reduce errors associated with the effects of illumination geometry. When used without the cosine corrector, upwelling radiance (UW) can be measured within a 25° field of view. The SKYE radiometers were calibrated based on their response to a National Institute of Standards and Technology (NIST) traceable light source in a uniform light source integrating sphere calibration system (OCL-61, Labsphere, Inc., North Sutton, NH). Each SKYE sensor was placed flush with the integrating sphere exit port with the light output maintained at 64,475 cd $m^{-2}$. The output of spectral radiance at the band centers of the green, red, red edge, and NIR bands was 793.5, 1236, 1333, and 1455 W $m^{-2}$ $sr^{-1}$ $nm^{-1}$, respectively. The output (in mV) of the SKYE sensors for each spectral band is proportional to the spectral radiance received. As part of the calibration process, the SKYE sensor was rotated 90° between readings to account for alignment bias in the calibration. An average of four alignment readings, in mV, for each waveband (e.g., green, red, red edge, or NIR) was recorded for each instrument. Each radiometer was calibrated with and without the cosine corrector at the start of the 2010 season and either with or without the cosine corrector based on their installation orientation for subsequent years. A

calibration coefficient was determined for each band based on the mV response to the integrating sphere output.

Sensors were calibrated before installation in the field and on completion of the field season. They were calibrated after their removal from the field in their post-field condition ("dirty") and again after being thoroughly cleaned ("clean") by wiping down the cosine corrector, removing spider silk in the sensor channels, and washing the filters. A marine sealant was applied around the cosine corrector to prevent water infiltration for the sensors used in the downwelling measurements so that the calibration values were relevant to the entire measurement period (otherwise, the periodic saturation and drying of sensors added noise that could not be corrected by the calibration procedure).

## Radiometric Measurements

All SKYE instruments were mounted 6 m above the ground on a tower (located in the middle of each field) in a nadir orientation such that the tower and its shadow were never in the field of view. For the irrigated fields, one downwelling and one upwelling instrument was installed. For the rainfed field, two upwelling instruments were installed 38 cm apart. With the row spacing being 76 cm, this instrument orientation provided one set of measurements above the row and one set of measurements between the rows. The lack of additional instruments did not allow for two upwelling radiometers at the irrigated sites. Responses from the radiometers were recorded every second between 0500 and 1900 h (CDT) from which 30 min averages were determined. Reflectance was determined by using a ratio of incoming irradiance and upwelling radiance collected by two four-band radiometers (see Data Processing for details).

Measurements of incoming and outgoing photosynthetically active radiation (PARin) were obtained using point quantum sensors (model LI-190, Li-Cor, Lincoln, NE). The ratio of the SKYE and PAR sensors mounted in the same orientation (i.e., ratio of downwelling instruments or ratio of upwelling instruments) was used as a quality control tool, with the assumption that the PAR sensor calibration did not change during the experiment. The ratio for each SKYE band and the respective PARin sensor determined near solar noon (1330 CDT) was compared to the previous day's ratio. Deviances of 50% or greater between these ratios were flagged and provide an indication of change for the calibration coefficients (see Data Processing for details).

## Data Processing

To remove short-term variation in the data due to rapidly changing irradiation as well as environmental conditions in which the radiometers were compromised by contaminants (e.g., birds, insects, or spiders), the spectral band radiometer responses, in mV, were averaged over a 30 min period. These 30-min average responses were converted to irradiance and radiance values using the appropriate band calibration coefficients. Dates flagged by SKYE/PARin ratios were examined to determine if the change was related to major differences in irradiation conditions or if an contaminant was involved. For periods where the ratio changed due to overcast sky conditions, the ratio returned to the values achieved under sunny conditions as illumination conditions changed. These points were also identified by examining the raw PARin values, which were much lower during cloudy conditions. Points where the ratio did not return to similar values after monitoring irradiation conditions were marked as the point where the "dirty" calibration coefficient for that particular band might be applied. In cases where the dirty calibration varied <5% from the pre-season calibration, only the initial calibration coefficient was used. In the instances where the difference between the dirty and clean calibrations was >5%, the errors were assumed to be introduced by contaminants. The date where the largest difference between the SKYE/PARin ratio from the previous day occurs was used as the point where the post-season dirty calibration was applied. This method is preferable over a gradual application of the corrected calibration from pre- to post-season coefficients since most changes occurred abruptly and could be identified as such in combination with the PAR albedo values. The contaminants consisted primarily of spider threads or insects blocking the sensor wells.

The 30-min averaged reflectance of spectral band "i" ($\rho_i$) was determined as the ratio of the 30-min average upwelling radiance [$R_{UW(\lambda)}$] and 30-min average downwelling irradiance [$I_{DW(\lambda)}$] (Eq. [1]).

$$\rho_i = [R_{UW(\lambda)} \times CC_{UW(\lambda)}] \times [I_{DW(\lambda)} \times CC_{DW(\lambda)}]^{-1} \quad [1]$$

where $CC_{UW(\lambda)}$ is the calibration coefficient at waveband λ for UW (mV) and $CC_{DW(\lambda)}$ for DW (mV). Photosynthetic photon flux density (PPFD, $\mu$mol $m^{-2}$ $s^{-1}$) was also calculated as the mV output times the Li-Cor supplied calibration coefficient from which daily PPFD were calculated (mol $m^{-2}$ $s^{-1}$).

The medians of the 30-min average reflectances between 10.5 and 15.5 h were used as the midday reflectance measurement to avoid skewing the data towards the minimum/maximum values of that day caused by drastic changes in the light conditions (overcast to sunny conditions) and to avoid bidirectional reflectance effects.

Vegetation lines and soil/residue lines were defined in the red vs. green and NIR vs. red reflectance spectral spaces. These lines define baselines from which vegetation growth and development could be qualitatively determined. Soil/residue lines were determined by collecting reflectance before planting when vegetation fractions were zero. Soil/stover/residue lines were determined by collecting reflectance after crop maturity and harvest when vegetation fractions were also zero but when fresh stover and residue were present. Vegetation lines (Gitelson et al., 2002b) were determined at peak vegetative stages when vegetation fraction exceeded 90%.

The VIs examined included normalized difference vegetation index, NDVI (Jordan, 1969), a modified version of the enhanced vegetation index, EVI2 (Liu and Huete, 1995; Jiang et al., 2008), and a two band version of the green visible atmospherically resistant index (VARI) (Gitelson et al., 2002a):

$$NDVI = (NIR - Red)/(NIR + Red) \quad [2]$$

$$EVI2 = 2.5 \times (NIR - Red)/(NIR + 2.4Red + 1) \quad [3]$$

$$VARI = (Green - Red)/(Green + Red) \quad [4]$$

The potential PARin values for each day (mol $m^{-2}$ $d^{-1}$; PARpotential) were determined using the method outlined in Weiss and Norman (1985). Deviations of PARin from

**Table 2. Percent change in radiometer sensitivity to a calibrated light source determined in the lab before installation and after removal from the site for the (A) 2010, (B) 2011, and (C) 2012 growing seasons (from May–October) for each spectral band of the seven radiometers tested. The post-season calibration included calibration before cleaning the sensor channels, filters, and cosine correctors ("dirty") and after cleaning these parts ("clean"). The view of the instrument is also listed: downward (D) or upward (U) facing.**

| | | | Green | | Red | | Red Edge | | Near infrared | |
|---|---|---|---|---|---|---|---|---|---|---|
| Instrument | Site | View | Dirty | Clean | Dirty | Clean | Dirty | Clean | Dirty | Clean |
| A. 2010 Growing season | | | | | | | | | | |
| A | 1 | U | –4.99 | –2.84 | –3.25 | 2.35 | –2.75 | –2.24 | –4.91 | –5.04 |
| B | 1 | D | –2.39 | –2.83 | –2.79 | 1.77 | –3.73 | 0.74 | –5.54 | –3.48 |
| C | 2 | U | –5.77 | –4.79 | –9.50 | 9.00 | –5.07 | –5.04 | –7.34 | –7.60 |
| D | 2 | D | –11.03 | –1.18 | –4.42 | 0.70 | –3.43 | –1.23 | –18.09 | –3.55 |
| E | 3 | U | –2.45 | –0.75 | –0.07 | 0.01 | –0.28 | –0.29 | –2.57 | –2.33 |
| F | 3 | D | –1.51 | 1.61 | –0.02 | 6.07 | 0.29 | 1.37 | –3.33 | 4.35 |
| G | 3 | D | –2.87 | 0.10 | –2.79 | 0.94 | –3.76 | –0.13 | –2.87 | 0.07 |
| B. 2011 Growing season | | | | | | | | | | |
| A | 1 | U | –5.94 | 1.49 | –3.56 | 0.74 | –0.67 | 2.02 | –5.88 | –4.54 |
| B | 1 | D | –23.87 | –0.03 | –3.39 | –1.12 | –2.2 | –0.5 | –8.08 | –3.00 |
| C | 2 | U | –2.79 | –0.28 | –0.19 | 0.29 | 0.84 | 1.12 | –2.4 | –1.89 |
| D | 2 | D | –10.02 | –1.38 | –5.23 | 0.36 | –1.57 | 0.89 | –8.29 | –3.92 |
| E | 3 | U | –7.26 | –2.4 | –1.76 | –0.32 | –1.18 | 0.67 | –3.41 | –1.67 |
| F | 3 | D | –12.00 | –1.67 | –3.79 | –1.74 | –3.18 | –0.67 | –6.09 | –3.32 |
| G | 3 | D | –5.94 | 1.49 | –3.56 | 0.74 | –0.67 | 2.02 | –5.88 | –4.54 |
| C. 2012 Growing season | | | | | | | | | | |
| A | 1 | U | –7.62 | –4.30 | –4.46 | –4.11 | –3.81 | –3.73 | –9.49 | –8.92 |
| B | 1 | D | –4.94 | –1.26 | –3.24 | –0.27 | –3.93 | –0.05 | –10.66 | –5.63 |
| C | 2 | U | –6.81 | –3.73 | –6.08 | –3.96 | –4.42 | –2.23 | –5.04 | –4.21 |
| D | 2 | D | –3.76 | 5.15 | –3.11 | 5.51 | –42.06 | –5.52 | –8.01 | –8.44 |
| E | 3 | U | –4.51 | –1.75 | –4.59 | –2.83 | –2.28 | –1.59 | –4.28 | –3.92 |
| F | 3 | D | –3.16 | –1.34 | –2.58 | 1.28 | –2.47 | 1.54 | –6.16 | –1.16 |
| G | 3 | D | –3.87 | –0.96 | –3.88 | –0.24 | –37.41 | –0.81 | –9.02 | –6.57 |

PARpotential were expressed as a percentage of PARpotential (%PARpotential) and provided an indication of the amount of direct light reaching the canopy where lower values indicate cloudy conditions:

$$\%\text{PARpotential} = \text{PARin}/\text{PARpotential} \quad [5]$$

Reflectances during days when %PARpotential was >70% were used in establishing the spectral space lines and examining the VI temporal behavior.

Vegetation fraction was retrieved from 2-D red vs. green spectral space as described in Gitelson et al. (2002b) as a distance between the soil and vegetation lines. The vegetation fraction determined from Nikon COOLPIX 5100 (Nikon Corp., Tokyo, Japan) camera data was based on the approach introduced by Woebbecke et al. (1995) which uses the brightness of the green and red bands to separate vegetation from soil and background residue. For details on the camera system see Sakamoto et al. (2012) and for details on the vegetation fraction estimation procedure see Gitelson et al. (2002a). Growing degree days (GDDs) were calculated following Method 2 (McMaster and Wilhelm, 1997) and using a base temperature of 10°C.

## RESULTS AND DISCUSSION

### Issues Associated with Long-Term Data Collection

The SKYE radiometers originally were calibrated by the manufacturer using pairs of sensors. The calibration used in this study did not require sensor pairs but instead provided an independent calibration of each sensor band (Markham et al., 1988; Walter-Shea and Biehl, 1990). If one instrument and/or sensor band in an upwelling/downwelling pair were to fail before the post-season calibration, data from the one functioning unit was still valuable and another calibrated sensor could be used as a replacement for the malfunctioning unit.

A summary of the changes in the calibration between the start and the end of the growing season (dirty) and between the start of the growing season and after cleaning the instruments (clean) is presented in Table 2. Overall the sensors deviated <10% (with some exceptions) between the calibrations collected before and after the growing season in their dirty state. The differences were reduced to <5% and no more than 10% once the sensors were cleaned. Differences between the dirty and clean conditions were usually less in the downwelling sensors since the cosine corrector prevented dust and insects from collecting in the sensor wells (Table 2). Large deviations between the preseason and postseason calibrations (e.g., 42% on Site 2, downwelling, red edge) may be of concern if only one calibration coefficient was applied to the data or if the change occurred gradually throughout the season. However, the application of a second calibration coefficient was generally all that was necessary because the data were generally impacted by rapid contamination of the sensor wells. As indicated for many of the bands in this study, the sensors were quite stable except when insects and/or spiders intruded into the sensor wells. For example, after cleaning, only 7% of the calibrations in the visible spectrum differed more than 5% from the pre-season calibration collected that year ($n = 63$). Reflectance in the NIR band was the most variable, 33% of the bands varied more than

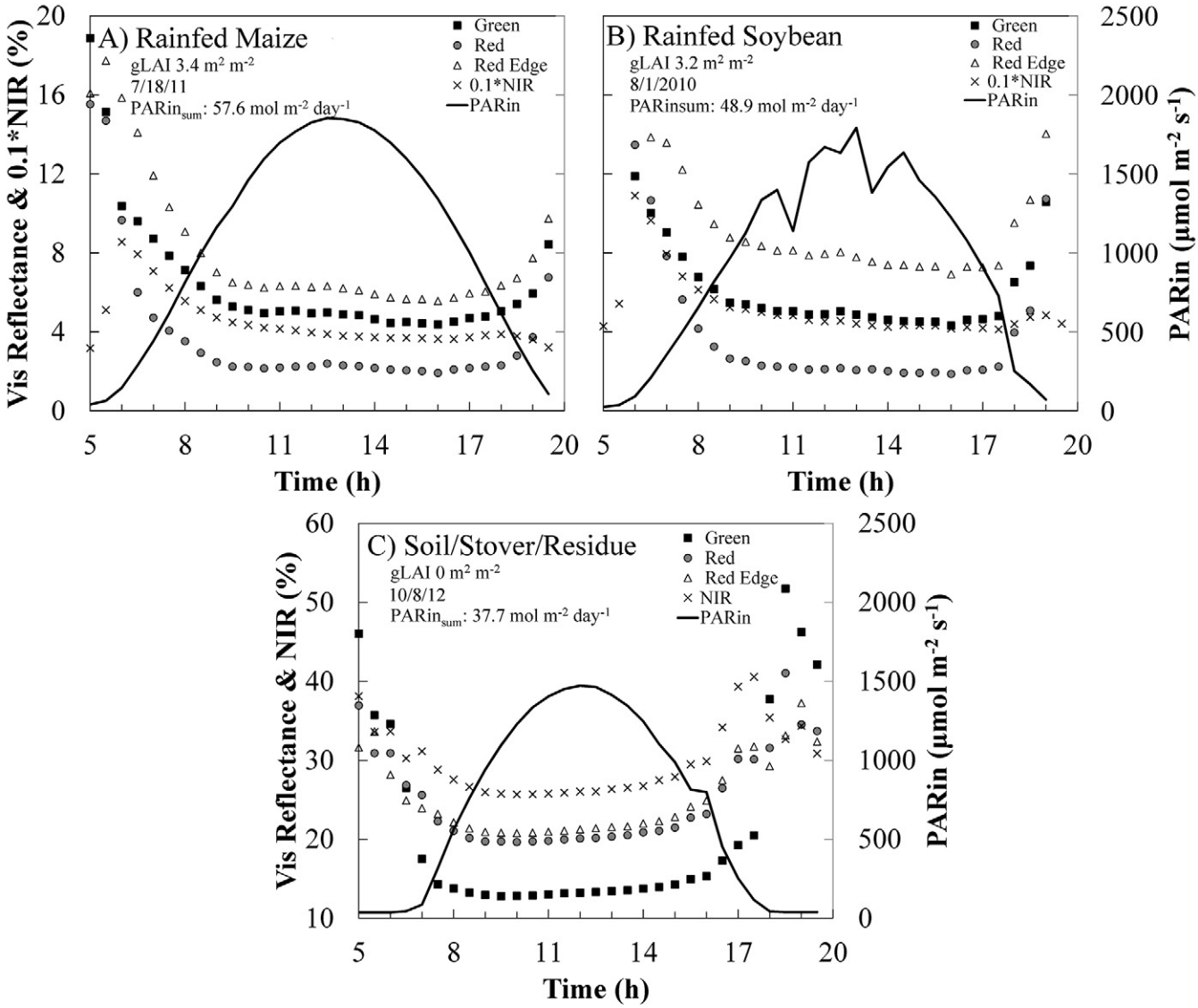


**Fig. 1. Diurnal behavior of reflectance during mostly cloud-free conditions for (A) maize with a green leaf area index (LAI) of 3.1 to 3.4 $m^2$ $m^{-2}$, (B) soybean with a green LAI of 3.0 to 3.5 $m^2$ $m^{-2}$, and (C) the non-growing season when green LAI is 0 $m^2$ $m^{-2}$. While all of the examples were taken from the rainfed field, similar behavior occurred at the other two sites. The figures used local time (CDT).**

5% between the pre- and post- season calibration after cleaning; however, none of the bands varied more than 9% ($n$ = 21). When the two sensors placed 38 cm apart were compared, there were only slight differences in slope of calibration (0.93–0.99) and coefficient of determination (0.977–0.997) for all four bands in the 2 yr examined for maize (2011) and soybean (2012). This indicates that the calibration procedure using the SKYE/PARin ratios to identify the application of the dirty calibration coefficient was reliable.

## Diurnal Reflectance

Canopy reflectances in all four bands changed dramatically with solar zenith angles when it exceeds 70° (e.g., just after sunrise and just before sunset) and attributed to higher specular reflectance contributions to the bidirectional reflectance factors (Norman et al., 1985). However, diurnal canopy reflectances varied little during periods of smaller (<70°) solar zenith angles (between 10.5 and 15.5 h CDT) and mostly clear skies for both maize (Fig. 1A) and soybean (Fig. 1B) especially when the canopy was at full cover (LAI above 3.0 $m^2$ $m^{-2}$). The minimum solar zenith angle for each day during the study ranged between 17.7° (DOY ~172) and 54.1° (DOY ~300).

On some occasions, the visible reflectance increased a little at solar noon compared to the reflectance collected 2.5 h before or after solar noon (Fig. 1A–1B). Of the midday reflectance measurements ($n$ = 1537) collected in 2010 through 2012 from all three fields, 243 midday reflectance measurements (15.8%) displayed a peak >5%. The average peak was 9.1% and the maximum peak was 23% greater at solar noon compared to the reflectance 2.5 h before or after.

Similar trends in diurnal reflectance have been reported before and have been attributed to the variations to specular reflectance from plant, residue, and soil, given the row structure and illumination angles (Ranson et al., 1985) or reduced shadowing when the sun is highest for the day so that the canopy appears brighter (Kimes, 1983). In addition, plant photoprotective mechanisms may play a role, decreasing absorption as plants reduce light striking the chloroplasts through leaf curling/folding and/or chloroplast avoidance movement (Zygielbaum et al., 2012). However, this explanation requires that plants are able to recover

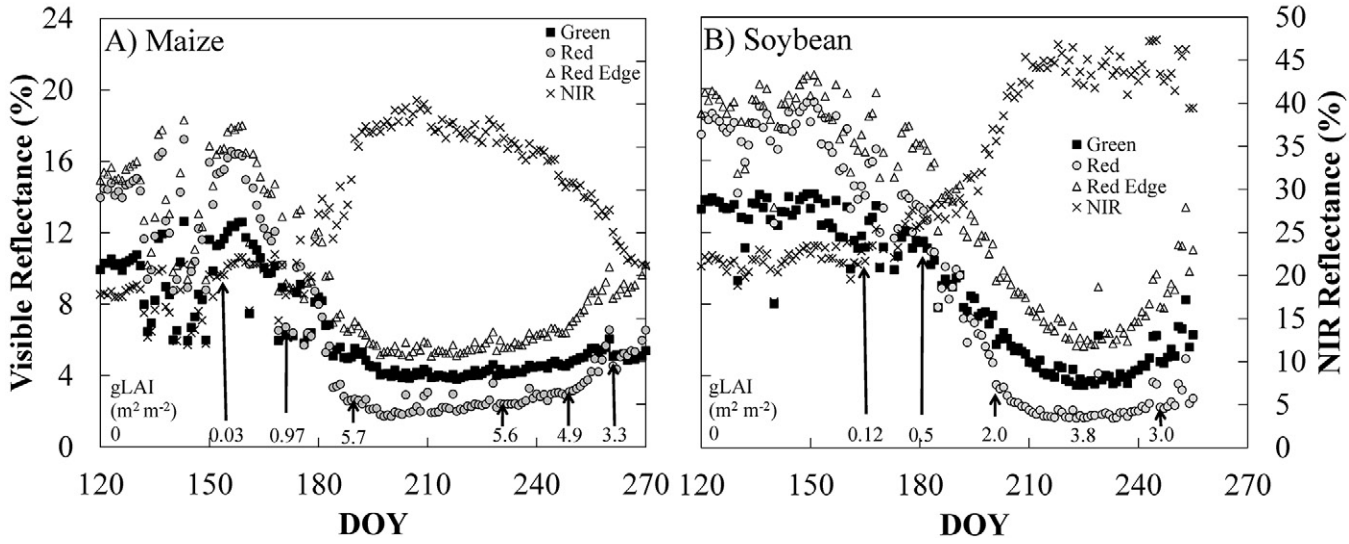


**Fig. 2. Temporal behavior of median reflectance of the visible and near infrared (NIR) wavebands collected between 1030 and 1530 CDT for (A) 2011 and (B) 2010. Crop green leaf area index (LAI) is indicated.**

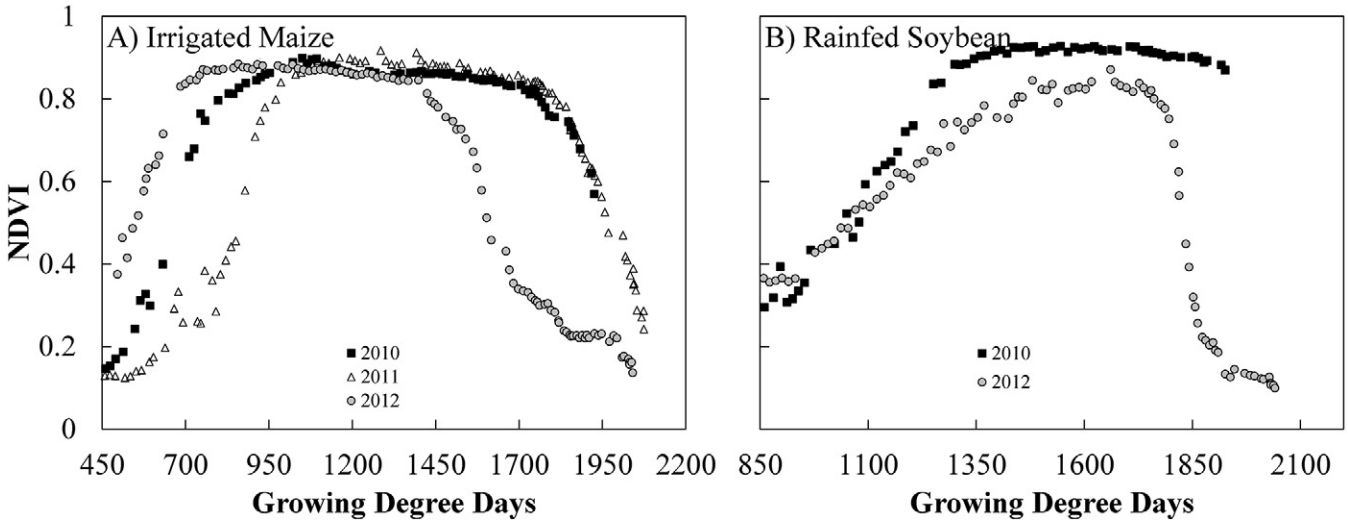


**Fig. 3. Temporal behavior of the normalized difference vegetation index (NDVI) for (A) maize and (B) soybean based on thermal time or growing degree days.**

after the peak at solar noon. These slight increases of reflectance occur more often when conditions were hot and dry and require further study. However, since the solar noon peak is uncommon (occurrence in 15.8% of samples), it is a rather minor component of the variation in the data set.

Diurnal canopy reflectance also varied little at the end of the growing season with low vegetation cover between 10.5 and 15.5 h when peak solar zenith angles were larger (Fig. 1C). Thus, the median reflectance ±2.5h from solar noon was minimally sensitive to short-term instant reflectance variability and effect of solar zenith angle variability. The median value of reflectances (i.e., midday reflectance) collected between 10.5 and 15.5 h was used to represent the daily canopy reflectance.

## Temporal Behavior of Reflectance during the Growing Season

Temporal behavior of the midday reflectance during the growing season was in accord with that reported in previous studies of maize and soybean (Verhulst et al., 2011; Foerster et al., 2012). As the plants developed and LAI increased, green, red, and red edge reflectances decreased due to an increase in total chlorophyll content (leaf chlorophyll content and LAI) and, thus, increase in absorption of photosynthetically active radiation, while NIR reflectance increased due to increase in LAI resulting in additional light scattering from leaves (Fig. 2). Of all the visible wavebands investigated, the red reflectance showed the greatest variation over the low range of LAI values; however, it saturated, or varied minimally, at LAIs >3 $m^2$ $m^{-2}$ (Fig. 2). As LAI increased, NIR reflectance peaked and was most variable around the time of tasseling in maize and maximal LAI in soybean.

In maize, during the early reproductive stages the NIR reflectance gradually decreased and then dropped rapidly during senescence. For soybean, the NIR reflectance remained almost invariant for about 30 d at midseason when LAI exceeded 3 $m^2$ $m^{-2}$, and began to decrease near the time of power failure on DOY 255 in 2010. For maize, grain maturity occurred around DOY 270 when LAI was below 2 $m^2$ $m^{-2}$. At this time, the green, red, and red edge reflectances increased rapidly.

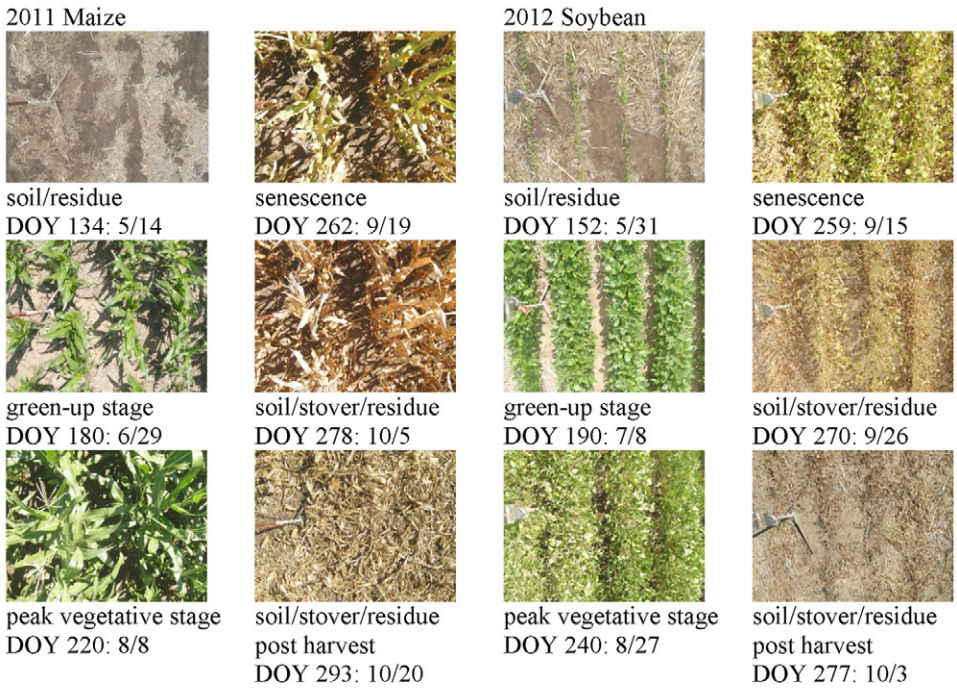


**Fig. 4. Images acquired from the rainfed fields for both maize and soybean. Images selected represent crop development stages identified in the spectral spaces.**

While the midday reflectance at each DOY removed most of the diurnal variation within a specific date, it did not remove all variations. Plants at the same development stage with the same LAI may have different reflectances due to different weather conditions affecting the light climate inside the canopy that caused deviations from the general trend in the temporal behavior. During periods of predominantly diffuse PAR (cloudy days), the light penetrates somewhat uniformly into the canopy from all directions. Self-shadowing decreases and therefore, a larger fraction of the upwelling radiation originates from "illuminated" vegetation and soil rather than from shaded components of the vegetation and soil when the direct beam dominates. Thus, a relative increase in crop canopy reflectance occurred during cloudy conditions (Schaaf and Strahler, 1993). These points can easily be removed from a data set by using %PARpotential to identify predominantly cloudy days.

Sensors set up for diurnal monitoring can capture reflectance on days of cloud cover when satellite- and airborne-based sensors cannot; however, the increase in reflectance due to the increase in the ratio of diffuse to direct light can result in an underestimation of a biophysical property when used in a model calibrated with reflectances collected under sunny conditions. Fortunately, these low light levels can be easily identified. While these data were excluded from analysis in this study, one could use incoming radiation as a parameter in developing these relationships. For example Peng and Gitelson (2011) used such a scheme for gross primary production estimation. Removing points during low light levels does reduce the size of the data set examined; however, this omission removes noise that can be explained while still preserving a more robust temporal data set. Even with these points removed due to low light conditions, a high temporal sensor can identify most changes in crop development stages compared to a system reliant entirely on satellite image acquisition and/or a field campaign which may sample only a few times per month.

## Vegetation Indices

The VIs were originally designed to capture the variation of reflectance in several spectral bands and reduce this information into a number that can be related to a property of the vegetation. The behavior of NDVI over thermal time (e.g., GDD) can provide indications of different physiological response (Fig. 3). For example, in 2012, severe drought caused both maize and soybean to senesce earlier, ~1400 and ~1750 GDD respectively, than previous years. Differences in the timing of crop planting can also be identified. For example, planting in 2011 was delayed due to the need to control volunteer maize caused by hail damage at the end of 2010 (Fig. 3A). Despite this difference in planting dates, the maize in the field matured and underwent senescence at approximately the same thermal time (~1750 GDD) for both years.

The VIs have also been used to monitor broad phenological changes and crop developmental stages such as soil/residue, green-up, peak vegetative, senescence, and soil/stover/residue stages (Fig. 4). Some, such as the visible atmospheric resistant index (VARI), were sensitive to reproductive structures (e.g., tassels) and thus can provide an indication of a specific crop phenological stage (Viña et al., 2004). The various VIs investigated had distinct temporal behavior (Fig. 5); however, each major crop developmental stage was not necessarily easy to identify. This was partially due to the design of many VIs, since one of the purposes of VIs was to identify stress. Thus, variation in the VIs caused by stress adds noise to the VI vs. DOY relationship. For example, it was quite difficult to identify the end of the peak vegetative stage in maize (Fig. 5), as well as beginning and end of this stage in soybean (Fig. 5b). The end of the soil/residue and start of the green up stages were distinguishable in maize, but was not clearly recognizable in soybean. Lastly, the start of the soil/stover/residue stage was easily recognizable in soybean, but not in maize. In systems where only a single crop is grown in a given year; this is not

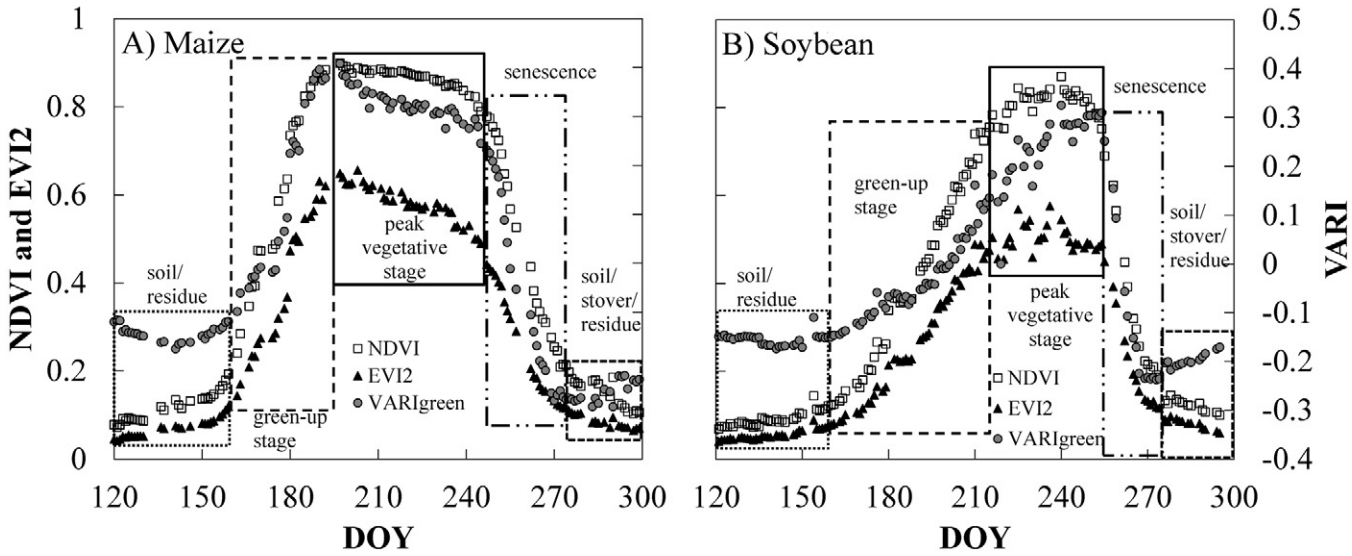


**Fig. 5. Temporal behavior of three vegetation indices for (A) maize (2011) and (B) soybean (2012). The broad crop development stages soil/residue, green-up, peak vegetative, senescence, and soil/stover/residue were identified.**

a problem because the day of year provides enough information to help identify the crop developmental stage. However, a user interested in identifying the crop developmental stage from an image in a region where multiple cropping is common will not be able to separate the green-up and senescence stage in the image. Therefore, an alternative method is necessary to identify crop development stages.

## Two-Dimensional Spectral Spaces

While the daily temporal behavior indicated similar patterns between reflectance bands in the visible spectral range, important additional information was extracted by examining spectral spaces, that is, relationships between reflectances in different spectral bands. Spectral spaces capitalize on the information content in different bands and, thus, sensitivities to vegetation physiological and crop developmental status.

The NIR vs. red relationships have been widely used (Ayyangar et al., 1980; Gobron et al., 1999; Broge and Leblanc, 2001). In this study, four distinct classes were identified in NIR/red spectral spaces for maize (Fig. 6A) and three for soybean (Fig. 6B). Stover was not distinguished in these relationships. This was because healthy leaves scatter more light in the NIR region than do soil and senesced leaves. Once the crop fully senesced or was harvested and the leaves were redistributed, the NIR reflectance reached its minimum. Another difference between maize and soybean occurred during the transition stages: green-up and senescence. For soybean, red reflectance changed at a rate approximately 1.6 times faster than NIR reflectance during green-up and nearly the same rate of change (1.4 times) during senescence. However, in maize this rate during the green-up stage was 6.4 times faster. In the senescence stage, NIR reflectances changed faster (1.3 times) than red reflectance, indicating that leaf architecture was changing faster than chlorophyll was degrading. Differences between maize and soybean in the NIR vs. red reflectance relationships can be explained by the different leaf structures and canopy architectures of these crops. Soybean leaf orientation is more horizontal than that of maize and chlorophyll content in the adaxial leaf surface is much higher than in maize leaves with the same total chlorophyll content. Thus, soybean scatters much more in the NIR range and its absorption is higher in the red.

Gitelson et al. (2002b) demonstrated that spectral spaces in visible ranges are useful in estimating vegetation fraction when using a data set of multiple crops with various soil backgrounds. However, when using a high temporal resolution data set, such as that provided by SKYE sensors, one can also monitor crop developmental stages of a crop remotely.

Up to five distinct vegetative growth stages were clearly identifiable in both maize and soybean using the red vs. green reflectance spectral space: soil/residue, green-up, peak vegetative, senescence, and soil/stover/residue stages (Fig. 4, 6C, 6D). The soil/residue lines were similar for both crops, differences in type of residue from the previous year notwithstanding, since the soil type and land management practices were similar. While most of the variations in reflectances at this stage were likely due to changes in soil moisture (Lobell and Asner, 2002), reflectance varied minimally during this stage.

Both crops had a similar green-up stage where both red and green reflectance rapidly and synchronously decreased. The red reflectance changed 1.9 times faster than green reflectance in maize and 1.6 times faster in soybean. When the vegetation fraction exceeded 0.7, the slope of the red reflectance vs. green reflectance relationship significantly decreased. The red reflectance was nearly invariant while the green reflectance changed for both maize and soybean. Thus, both crops had a distinct "vegetation line" (Gitelson et al., 2002b).

A major change in the red vs. green reflectance behavior occurred at the onset of senescence: the green reflectance remained relatively low (~6% in maize and ~9% in soybean) and virtually invariant, while red reflectance increased drastically (from 3–12% in maize and to 15% in soybean). Thus, this crop stage can be clearly identified. Both crops had a similar soil/stover/residue line that was offset from the soil/residue line at the start of the growing season. In minimum-till management systems, fresh stover and residue have a distinctly different spectral characteristic from pre-planting conditions. Fresh stover and residue is usually brighter than the background soil. After harvest the remaining residue will

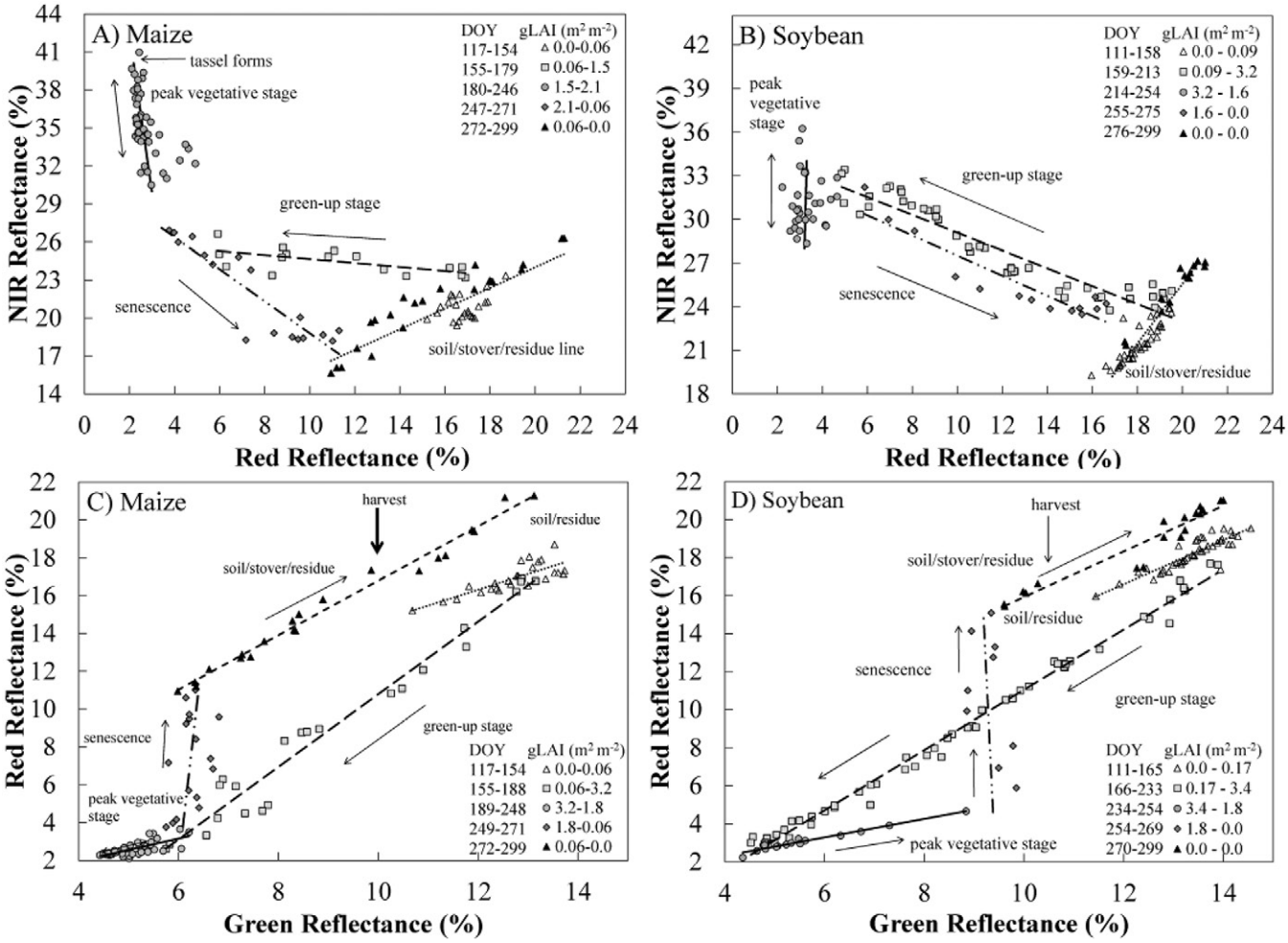


**Fig. 6. Two-dimensional spectral spaces formed by median midday rainfed (A,C) maize (2011) and (B,D) soybean (2012) reflectances when $PAR_{in}$ was >70% of PAR potential. Ranges of leaf area index (LAI) are shown. Maximum LAI for maize (3.49 $m^2$ $m^{-2}$) was reached on DOY 216 and for soybean (3.31 $m^2$ $m^{-2}$) on DOY 230.**

begin to decompose and become better incorporated into the soil, thus reducing its reflectance (Streck et al., 2002). For this reason, the soil/stover/residue line appeared higher and longer than the soil/residue line. By the beginning of the next growing season, reflectances will overlay onto the soil/residue line of the previous year with slight variations (Fig. 7A).

Noise identified in the temporal behavior of VIs (Fig. 5B) was not incorporated into the red vs. green reflectance relationship and the peak vegetative stage was clearly defined (Fig. 6C), thus providing benefit over using VIs. A second benefit is that end users who wish to identify the crop developmental stage from satellite imagery without any ancillary data can use the red vs. green relationship because it was possible to identify the stage based on the location of the point in spectral space. For example, using the 7-field years of data collected using the SKYE sensors, most of the points identified in each crop stage can be found in a specific region in the red vs. green spectral space (Fig. 7). This is despite differences in crop management (e.g., irrigated vs. rainfed), hybrids, and climatic conditions (e.g., there was a severe drought in 2012). Users working with satellite or aerial imagery may benefit from being able to identify the probability of a pixel landing within a crop developmental stage. This approach will assist in identifying regions in an image where double cropping occurs without relying on multiple image acquisitions.

We also tested the technique for estimating vegetation fraction using spectral spaces in the visible range (Gitelson et al., 2002b). It was found that the technique is able to estimate vegetation fraction with root mean square errors of 0.071 and 0.064 in maize and soybean, respectively (Fig. 8). The technique traditionally uses regional or local soil and vegetation lines collected for several years to be representative of the region and crops studied. In this study, soil and vegetation lines collected for only 1 yr were used; thus, further study is needed to assess uncertainties in the estimation of vegetation fraction using spectral spaces.

## CONCLUSIONS

This study investigated the utility of daily remote sensing monitoring of crop developments using 4-band radiometers throughout the growing season. Through continuous monitoring, diurnal and seasonal behavior of reflectance was characterized in maize and soybean. This study found that the median midday reflectance was a valid and stable measure of reflectance for maize and soybean under varying weather conditions; however, further research is necessary to identify the source of the peaks in reflectance at mid-day in a small but sizeable number of observations.

Two-dimensional spectral spaces, specifically, relationships between reflectances in visible spectral range (red vs. green), were useful for detecting crop developmental stages in maize and

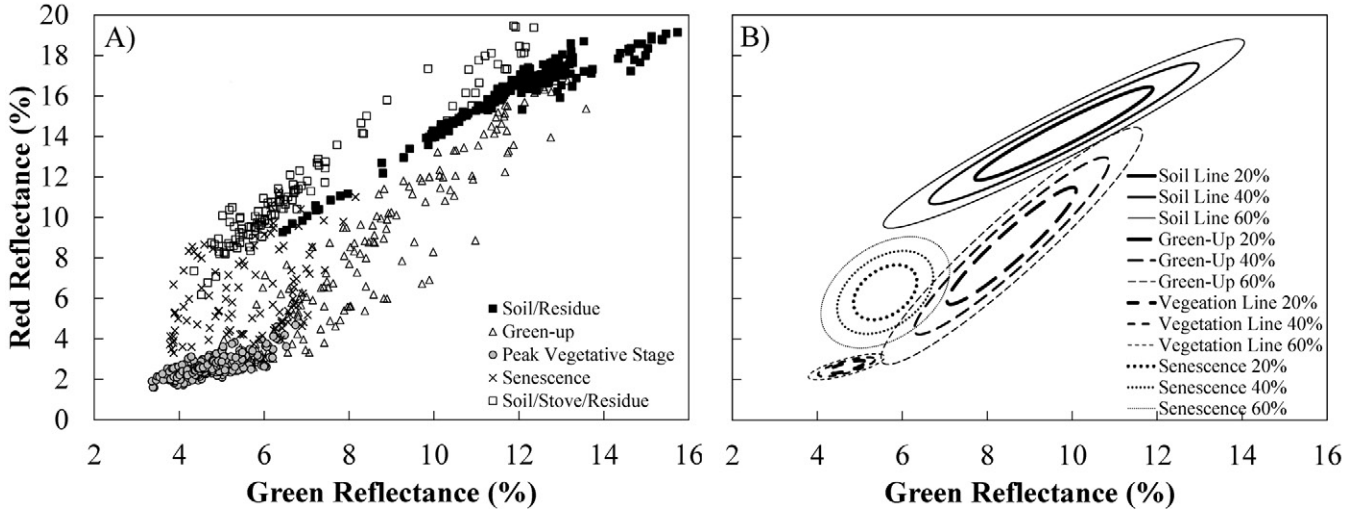


**Fig. 7. (A) The red vs. green reflectance relationships for 7-field years of observation using the high temporal data collected over maize divided into the five categories identified in Fig. 5. (B) Zones of probability for the soil line, green-up stage, vegetation line, and senescence stage are represented by ellipses encompassing 20, 40, and 60% of the daily values collected over maize. The soil line includes both the soil/residue and soil/stover/residue categories from panel A.**

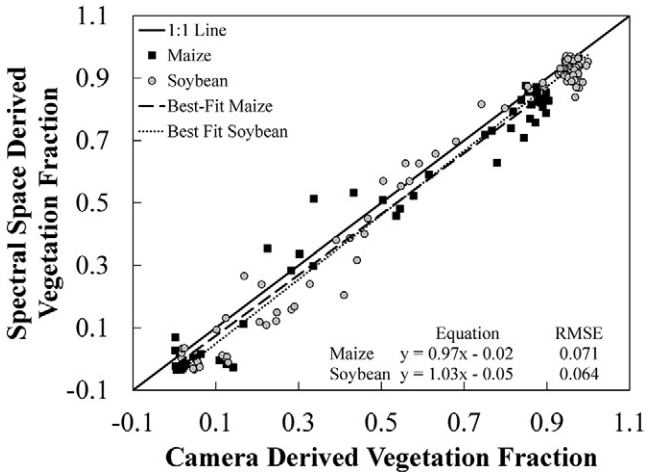


**Fig. 8. Vegetation fraction for both maize and soybean estimated using a digital camera vs. vegetation fraction retrieved from spectral spaces.**

soybean. Using the changes in sensitivity with crop development of each individual spectral band, five distinct vegetative growth stages were identified in both maize and soybean. Future studies should be directed towards determining whether these stages can be discerned in other species or crop types and if the patterns identified are similar to those found in this study. A method of using this information in an operational sense should also be explored. In addition, the distance between soil and vegetation lines in the 2-D red vs. green spectral space can be used as a proxy of vegetation fraction. Two-dimensional spectral spaces bring additional information not contained in VIs. Further studies should focus on understanding the value of identifying the developmental stage in multiple cropping systems and vegetation fraction estimation.

## ACKNOWLEDGMENTS

We appreciate the efforts provided by Dave Scoby in determining the green LAI in maize and soybean. We also appreciate the support and use of facilities and equipment provided by the Center for Advanced Land Management Information Technologies (CALMIT) and the Carbon Sequestration Program, University of Nebraska-Lincoln through the Office of Science (BER) U.S. Department of Energy Grant no. DE-FG02-03ER63639. We would also like to thank Toshihiro Sakamoto for the use of his digital cameras for the purpose of illustrating the phenological stages.

## REFERENCES

Abendroth, L.J., R.W. Elmore, M.J. Boyeer, and S.K. Marlay. 2011. Corn growth and development. Iowa State Univ. Ext., Ames.

Ayyangar, R.S., P.P. Nagaeshwara Rao, and K.R. Rao. 1980. Crop cover and crop phenological information from red and infrared spectral responses. J. Indian Soc. Photo-Interpretation Rem. Sens. 8:23–29.

Betancourt, J.L., M.D. Schwartz, D.D. Breshears, D.R. Cayan, M.D. Dettinger, D.W. Inouye et al. 2005. Implementing a U.S. National Phenology Network. Eos, Transactions American Geophysical Union 86:539.

Broge, N.H., and E. Leblanc. 2001. Comparing prediction power and stability of broadband and hyperspectral vegetation indices for estimation of green leaf area index and canopy chlorophyll density. Remote Sens. Environ. 76:156–172.

Cleary, B.D., and R.H. Waring. 1969. Temperature: Collection of data and its analysis for the interpretation of plant growth and distribution. Can. J. Bot. 47:167–173. doi:10.1139/b69-020

Crist, E.P., and R.J. Kauth. 1986. The tasseled cap de-mystified. Photogramm. Eng. Remote Sens. 52:81–86.

de Souza, E.G., P.C. Scharf, and K.A. Sudduth. 2010. Sun position and cloud effects on reflectance and vegetation indices of corn. Agron. J. 102:734–744. doi:10.2134/agronj2009.0206

Eklundh, L., H. Jin, P. Schubert, R. Guzinski, and M. Heliasz. 2011. An optical sensor network for vegetation phenology monitoring and satellite data calibration. Sensors (Basel Switzerland) 11:7678–7709. doi:10.3390/s110807678

Foerster, S., K. Kaden, M. Foerster, and S. Itzerott. 2012. Crop type mapping using spectral–temporal profiles and phenological information. Comput. Electron. Agric. 89:30–40. doi:10.1016/j.compag.2012.07.015

Gamon, J.A., and B. Bond. 2013. Effects of irradiance and photosynthetic downregulation on the photochemical reflectance index in douglas-fir and ponderosa pine. Remote Sens. Environ. 135:141–149. doi:10.1016/j.rse.2013.03.032

Gitelson, A.A., Y.J. Kaufman, R. Stark, and D. Rundquist. 2002a. Novel algorithms for remote estimation of vegetation fraction. Remote Sens. Environ. 80:76–87. doi:10.1016/S0034-4257(01)00289-9

Gitelson, A.A., R. Stark, U. Grits, D. Rundquist, Y. Kaufman, and D. Derry. 2002b. Vegetation and soil lines in visible spectral space: A concept and technique for remote estimation of vegetation fraction. Int. J. Remote Sens. 23:2537–2562. doi:10.1080/01431160110107806

Gobron, N., B. Pinty, M. Verstraete, and Y. Govaerts. 1999. The MERIS Global Vegetation Index (MGVI): Description and preliminary application. Int. J. Remote Sens. 20:1917–1927. doi:10.1080/014311699212542

Goodin, D.G., and G.M. Henebry. 1997. A technique for monitoring ecological disturbance in tallgrass prairie using seasonal NDVI trajectories and a discriminant function mixture model. Remote Sens. Environ. 61:270–278. doi:10.1016/S0034-4257(97)00043-6

Hansen, M., R. DeFries, C. Dimiceli, C. Huang, R. Sohiberg, X. Zhan, and J. Townshend. 1998. Red and infrared space partitioning for detecting land cover change. IGARSS'98. Sensing and Managing the Environment. 1998 IEEE International Geoscience and Remote Sensing. Symposium Proceedings. (Cat. no.98CH36174) 5:2512–2514.

Hanway, J.J. 1963. Growth stages of corn (*Zea mays* L.). Agron. J. 55:487–492. doi:10.2134/agronj1963.00021962005500050024x

Huete, A.R. 2012. Vegetation indices, remote sensing and forest monitoring. Geography Compass 6:513–532. doi:10.1111/j.1749-8198.2012.00507.x

Hufkens, K., M. Friedl, O. Sonnentag, B.H. Braswell, T. Milliman, and A.D. Richardson. 2012. Linking near-surface and satellite remote sensing measurements of deciduous broadleaf forest phenology. Remote Sens. Environ. 117:307–321. doi:10.1016/j.rse.2011.10.006

Idso, S.B., and C.T. de Wit. 1970. Light relations in plant canopies. Appl. Opt. 9:177–184. doi:10.1364/AO.9.000177

Jiang, Z., A.R. Huete, K. Didan, and T. Miura. 2008. Development of a two-band enhanced vegetation index without a blue band. Remote Sens. Environ. 112:3833–3845. doi:10.1016/j.rse.2008.06.006

Jordan, C.F. 1969. Derivation of leaf-area index from quality of light on the forest floor. Ecology 50:663–666. doi:10.2307/1936256

Kimes, D.S. 1983. Dynamics of directional reflectance factor distributions for vegetation canopies. Appl. Opt. 22:1364–1372. doi:10.1364/AO.22.001364

Liang, S., C.J. Shuey, A.L. Russ, H. Fang, M. Chen, C.L. Walthall et al. 2003. Narrowband to broadband conversions of land surface albedo: II. Validation. Remote Sens. Environ. 84:25–41. doi:10.1016/S0034-4257(02)00068-8

Liu, H.Q., and A.R. Huete. 1995. A feedback based modification of the NDVI to minimize canopy background and atmospheric noise. IEEE Trans. Geosci. Rem. Sens. 33:457–465. doi:10.1109/36.377946

Lobell, D.B., and G.P. Asner. 2002. Moisture effects on soil reflectance. Soil Sci. Soc. Am. J. 66:722–727. doi:10.2136/sssaj2002.0722

Markham, B.L., F.M. Wood, Jr., and S.P. Ahmad. 1988. Radiometric calibration of the reflective bands of NS001-Thematic Mapper Simulator (TMS) and Modular Multispectral Radiometers (MMR). Proc. SPIE 0924:96–108. doi:10.1117/12.945677

McMaster, G.S., and W.W. Wilhelm. 1997. Growing degree-days: One equation, two interpretations. Agric. For. Meteorol. 87:291–300. doi:10.1016/S0168-1923(97)00027-0

Norman, J.M., J. Welles, and E. Walter. 1985. Contrasts among bidirectional reflectance of leaves, canopies, and soils. IEEE Trans. Geosci. Rem. Sens. GE-23:659–667. doi:10.1109/TGRS.1985.289384

Peng, Y., and A.A. Gitelson. 2011. Application of chlorophyll-related vegetation indices for remote estimation of maize productivity. Agric. For. Meteorol. 151:1267–1276. doi:10.1016/j.agrformet.2011.05.005

Pinter, P.J. 1986. Effect of dew on canopy reflectance and temperature. Remote Sens. Environ. 19:187–205. doi:10.1016/0034-4257(86)90071-4

Ramsey, E.W. 1995. Monitoring flooding in coastal wetlands by using radar imagery and ground-based measurements. Int. J. Remote Sens. 16:2495–2502. doi:10.1080/01431169508954571

Ranson, K.J., C.S.T. Daughtry, L.L. Biehl, and M.E. Bauer. 1985. Sun-view angle effects on reflectance factors of corn canopies. Remote Sens. Environ. 18:147–161. doi:10.1016/0034-4257(85)90045-8

Richardson, A.D., B.H. Braswell, D.Y. Hollinger, J.P. Jenkins, and S.V. Ollinger. 2009. Near-surface remote sensing of spatial and temporal variation in canopy phenology. Ecol. Appl. 19:1417–1428. doi:10.1890/08-2022.1

Ryu, Y., D.D. Baldocchi, J. Verfaillie, S. Ma, M. Falk, I. Ruiz-Mercado, T. Hehn, and O. Sonnentag. 2010. Testing the performance of a novel spectral reflectance sensor, built with light emitting diodes (LEDs), to monitor ecosystem metabolism, structure and function. Agric. For. Meteorol. 150:1597–1606. doi:10.1016/j.agrformet.2010.08.009

Sakamoto, T., A.A. Gitelson, A.L. Nguy-Robertson, T.J. Arkebauer, B.D. Wardlow, A.E. Suyker et al. 2012. An alternative method using digital cameras for continuous monitoring of crop status. Agric. For. Meteorol. 154–155:113–126. doi:10.1016/j.agrformet.2011.10.014

Schaaf, C.B., and H. Strahler. 1993. Solar zenith angle effects on forest canopy hemispherical reflectances calculated with a geometric-optical bidirectional reflectance model. IEEE Trans. Geosci. Rem. Sens. 31:921–927. doi:10.1109/36.239916

Sivanpillai, R., and B.E. Ewers. 2013. Relationship between sagebrush species and structural characteristics and Landsat Thematic Mapper data. Appl. Veg. Sci. 16:122–130. doi:10.1111/j.1654-109X.2012.01207.x

Soudani, K., G. Hmimina, N. Delpierre, J.-Y. Pontailler, M. Aubinet, D.J. Bonfil et al. 2012. Ground-based network of NDVI measurements for tracking temporal dynamics of canopy structure and vegetation phenology in different biomes. Remote Sens. Environ. 123:234–245. doi:10.1016/j.rse.2012.03.012

Squires, J.R., N.J. DeCesare, L.E. Olson, J.A. Kolbe, M. Hebblewhite, and S.A. Parks. 2013. Combining resource selection and movement behavior to predict corridors for Canada lynx at their southern range periphery. Biol. Conserv. 157:187–195. doi:10.1016/j.biocon.2012.07.018

Streck, N.A., D. Rundquist, and J. Connot. 2002. Estimating residual wheat dry matter from remote sensing measurements. Photogramm. Eng. Remote Sens. 68:1193–1201.

Suyker, A.E., S.B. Verma, G.G. Burba, and T.J. Arkebauer. 2005. Gross primary production and ecosystem respiration of irrigated maize and irrigated soybean during a growing season. Agric. For. Meteorol. 131:180–190. doi:10.1016/j.agrformet.2005.05.007

Verhulst, N., B. Govaerts, V. Nelissen, K.D. Sayre, J. Crossa, D. Raes, and J. Deckers. 2011. The effect of tillage, crop rotation and residue management on maize and wheat growth and development evaluated with an optical sensor. Field Crops Res. 120:58–67. doi:10.1016/j.fcr.2010.08.012

Verma, S.B., A. Dobermann, K.G. Cassman, D.T. Walters, J.M. Knops, T.J. Arkebauer et al. 2005. Annual carbon dioxide exchange in irrigated and rainfed maize-based agroecosystems. Agric. For. Meteorol. 131:77–96. doi:10.1016/j.agrformet.2005.05.003

Viña, A., A.A. Gitelson, D.C. Rundquist, G.P. Keydan, B. Leavitt, and J. Schepers. 2004. Monitoring maize (L.) phenology with remote sensing. Agron. J. 96:1139–1147. doi:10.2134/agronj2004.1139

Walter-Shea, E.A., and L.L. Biehl. 1990. Measuring vegetation spectral properties. Remote Sens. Rev. 5:179–205. doi:10.1080/02757259009532128

Weiss, A., and J.M. Norman. 1985. Partitioning solar radiation into direct and diffuse, visible and near-infrared components. Agric. For. Meteorol. 34:205–213. doi:10.1016/0168-1923(85)90020-6

Woebbecke, D.M., G.E. Meyer, K. Von Bargen, and D.A. Mortensen. 1995. Color indices for weed identification under various soil residue and lighting conditions. Trans. ASAE 38:259–269.

Zarco-Tejada, P. 2000. Chlorophyll fluorescence effects on vegetation apparent reflectance II. laboratory and airborne canopy-level measurements with hyperspectral data. Remote Sens. Environ. 74:596–608. doi:10.1016/S0034-4257(00)00149-8

Zygielbaum, A.I., T.J. Arkebauer, E.A. Walter-Shea, and D.L. Scoby. 2012. Detection and measurement of vegetation photoprotection stress response using PAR reflectance. Isr. J. Plant Sci. 60:37–47. doi:10.1560/IJPS.60.1-2.37